Conditions for Photonic Bandgaps in Two-Dimensional Materials

Alexander M. Holmes[1, a)] and George W. Hanson[1, b)]
Department of Electrical Engineering, University of Wisconsin-Milwaukee
3200 N. Cramer St., Milwaukee, Wisconsin 53211, USA

(Dated: 1 December 2020)

Conditions that define the spectral location of bandgaps in the quasi-transverse magnetic surface plasmon polariton modal dispersion for 2D/quasi-2D materials with a tensor response function, embedded in a simple isotropic medium are obtained. In the isotropic case, transverse magnetic surface plasmon polariton modes propagate if the surface conductivity is inductive. However, in the anisotropic case considered here, we find that quasi-transverse magnetic modes are supported by surfaces with an inductive effective conductivity seen by the wave along the direction of propagation (written as a weighted sum of the diagonal elements). Examples of natural anisotropic 2D/quasi-2D materials are presented to demonstrate the effectiveness of the method.

I. INTRODUCTION

Surface Plasmon Polaritons (SPPs) guided by a single interface between dielectric and metal are extremely important in the field of optics as they can overcome the diffraction limit[1]. Since the discovery of graphene[2,3] and other two-dimensional materials such as the transition metal dichalchogenides (TMDs)[4], transition metal oxides (TMOs)[5–7], boron nitride (BN)[8–10], black phosphorous (BP)[11–15], borophene[16], and α-MoO_3[17], research in this area has continued to grow as many of these materials have useful conductive properties, making it possible for them to support robust SPPs with large confinement and propagation length. In addition, the study of quasi-2D van der Waals heterostructures consisting of two or more of these materials in parallel, is of growing popularity[18–24]. In contrast to artificial metasurfaces[25–28], where design parameters such as the unit cell and periodicity govern behavior, interactions at the atomic level are the driving factor behind the unique optical and electronic properties of natural 2D/quasi-2D materials.

For both artificial and natural materials, a tensor response function can arise. Of particular interest are materials and metasurfaces with anisotropic qualities due to asymmetry (i.e., time-reversal and/or translational) which are especially attractive in applications sensitive to polarization and/or the propagation direction. Translational asymmetry is found naturally in the crystal lattice of black phosphorous and in patterned isotropic materials[29–31]. Time reversal symmetry is broken in gapped dirac materials pumped with an AC plane wave[32] and in materials biased with an external magnetic field[33–36].

The novel properties of SPPs guided at the surface of two-dimensional materials are heavily dependent on the conductivity. In addition to low loss, a strong SPP response is obtained when the diagonal elements of the conductivity tensor are an order of magnitude greater than the conductance quantum[37] $G_0 = 2e^2/h$ where e, h denote the fundamental charge unit and Planck's constant respectively. In the isotropic case, the capacitive/inductive nature of the conductivity, determined very simply by the sign of the imaginary part, governs the propagation of transverse-electric/magnetic (TE/TM) SPP modes[38,39] where transverse is defined with respect to the propagation direction. In the time convention $\exp(-i\omega t)$, assumed throughout this work, a capacitive/inductive local, dispersive conductivity has $\mathrm{Im}\{\sigma(\omega)\} \lessgtr 0$ and $\mathrm{Re}\{\sigma(\omega)\} > 0$ with the real part accounting for loss. This makes characterizing the conductivity and predicting TE/TM SPP mode propagation with respect to operational frequency rather straightforward. In the anisotropic case, the SPP modes are hybrid, generally having some combination of TE and TM polarizations. These hybrid modes are commonly referred to as quasi-TE/TM (QTE/QTM) depending on which polarization is dominant. Moreover, it is not clear a priori what conditions on the response tensor define a capacitive/inductive surface, or even if that concept is relevant for the propagation of QTE/QTM modes. As such, it is not known where bandgaps will arise.

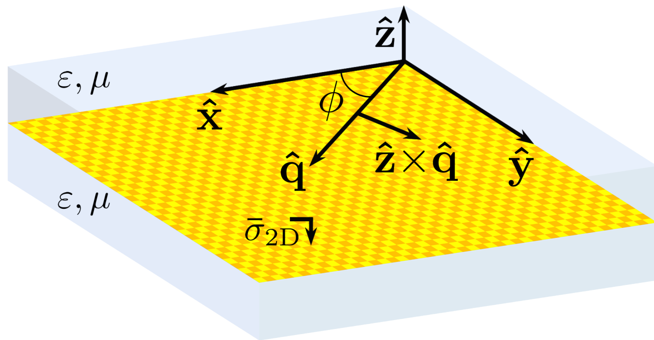

FIG. 1. Anisotropic two-dimensional material characterized by surface conductivity tensor $\bar{\sigma}_{2D}$ embedded in a simple, isotropic medium characterized by permittivity ε and permeability μ. Quasi-TM SPP modes supported by the structure have a dominant magnetic field component along $\hat{\mathbf{z}} \times \hat{\mathbf{q}}$ and propagate at the surface in the $\hat{\mathbf{q}}$ direction. The angle $\hat{\mathbf{q}}$ makes with $\hat{\mathbf{x}}$ is denoted ϕ.

The goal of this manuscript is to present a simple and reliable analytical method to determine when QTM modes are allowed to propagate, and the spectral location (i.e., temporal and spacial) of bandgaps in the QTM SPP dispersion associated with local, dispersive, anisotropic two-dimensional

a)Electronic mail: holmesam@uwm.edu
b)Electronic mail: george@uwm.edu

materials. Here, we show that a surface with an inductive effective conductivity (defined below) supports the propagation of QTM modes. We characterize the material response by considering the effective conductivity seen by the wave along the propagation direction, written as a weighted sum of the diagonal elements; the sign of which determines whether the material is inductive. We provide mathematical and physical arguments in section II to justify the validity of the method, and provide two examples in section III.

II. FORMULATION

In the following, we consider a local, dispersive, anisotropic two-dimensional material embedded in a simple, isotropic medium characterized by permittivity ε and permeability μ, depicted in Fig. 1. The surface conductivity, represented generally in the standard (Cartesian) basis, is

$$\bar{\sigma}_s(\omega) = \begin{pmatrix} \sigma_{\hat{\mathbf{x}}\hat{\mathbf{x}}}(\omega) & \sigma_{\hat{\mathbf{x}}\hat{\mathbf{y}}}(\omega) \\ \sigma_{\hat{\mathbf{y}}\hat{\mathbf{x}}}(\omega) & \sigma_{\hat{\mathbf{y}}\hat{\mathbf{y}}}(\omega) \end{pmatrix}, \tag{1}$$

with the condition $\sigma_{\hat{\mathbf{x}}\hat{\mathbf{y}}}(\omega) = -\sigma_{\hat{\mathbf{y}}\hat{\mathbf{x}}}(\omega)$. For convenience, we work in a coordinate system spanned by the set of orthonormal basis vectors $\{\hat{\mathbf{q}}, \hat{\mathbf{z}}, \hat{\mathbf{z}} \times \hat{\mathbf{q}}\}$ where $\mathbf{q}$ denotes the in-plane momentum. The representation of the surface conductivity in this frame is

$$\bar{\sigma}(\omega, \phi) = \mathbf{U}^{-1}(\phi) \cdot \bar{\sigma}_s(\omega) \cdot \mathbf{U}(\phi), \tag{2}$$

where

$$\mathbf{U}(\phi) = \begin{pmatrix} \cos(\phi) & -\sin(\phi) \\ \sin(\phi) & \cos(\phi) \end{pmatrix}, \tag{3}$$

with ϕ denoting the angle of propagation (i.e., the angle $\mathbf{q}$ makes with $\hat{\mathbf{x}}$). Expanding the transformation in (2) results in

$$\bar{\sigma}(\omega, \phi) = \begin{pmatrix} \sigma_{\hat{\mathbf{q}}\hat{\mathbf{q}}}(\omega, \phi) & \sigma_{\hat{\mathbf{q}}(\hat{\mathbf{z}}\times\hat{\mathbf{q}})}(\omega, \phi) \\ \sigma_{(\hat{\mathbf{z}}\times\hat{\mathbf{q}})\hat{\mathbf{q}}}(\omega, \phi) & \sigma_{(\hat{\mathbf{z}}\times\hat{\mathbf{q}})(\hat{\mathbf{z}}\times\hat{\mathbf{q}})}(\omega, \phi) \end{pmatrix} \tag{4}$$

where

$$\sigma_{\hat{\mathbf{q}}\hat{\mathbf{q}}} = \sigma_{\hat{\mathbf{x}}\hat{\mathbf{x}}}(\omega)\cos^2(\phi) + \sigma_{\hat{\mathbf{y}}\hat{\mathbf{y}}}(\omega)\sin^2(\phi), \tag{5}$$
$$\sigma_{\hat{\mathbf{q}}(\hat{\mathbf{z}}\times\hat{\mathbf{q}})} = \sigma_{\hat{\mathbf{x}}\hat{\mathbf{y}}}(\omega) + \delta\sigma_s(\omega)\cos(\phi)\sin(\phi), \tag{6}$$
$$\sigma_{(\hat{\mathbf{z}}\times\hat{\mathbf{q}})\hat{\mathbf{q}}} = -\sigma_{\hat{\mathbf{x}}\hat{\mathbf{y}}}(\omega) + \delta\sigma_s(\omega)\cos(\phi)\sin(\phi), \tag{7}$$
$$\sigma_{(\hat{\mathbf{z}}\times\hat{\mathbf{q}})(\hat{\mathbf{z}}\times\hat{\mathbf{q}})} = \sigma_{\hat{\mathbf{x}}\hat{\mathbf{x}}}(\omega)\sin^2(\phi) + \sigma_{\hat{\mathbf{y}}\hat{\mathbf{y}}}(\omega)\cos^2(\phi), \tag{8}$$

and $\delta\sigma_s = \sigma_{\hat{\mathbf{y}}\hat{\mathbf{y}}} - \sigma_{\hat{\mathbf{x}}\hat{\mathbf{x}}}$.

The boundary conditions on the electric and magnetic fields $\mathbf{E}, \mathbf{H}$ at the interface ($z = 0$) in the spacial transform domain with respect to x, y are

$$\hat{\mathbf{z}} \times \left[\mathbf{E}\left(\mathbf{q}, 0^+\right) - \mathbf{E}\left(\mathbf{q}, 0^-\right)\right] = \mathbf{0}, \tag{9}$$
$$\hat{\mathbf{z}} \times \left[\mathbf{H}\left(\mathbf{q}, 0^+\right) - \mathbf{H}\left(\mathbf{q}, 0^-\right)\right] = \bar{\sigma} \cdot \mathbf{E}\left(\mathbf{q}, 0^+\right), \tag{10}$$

and lead to the recovery of the SPP dispersion relation

$$\det\left(2\bar{\mathbf{Y}} - \bar{\sigma}\right) = 0 \tag{11}$$

where $\mathbf{q}$ is preserved across the interface and $\bar{\mathbf{Y}}$ is defined in the appendix. Explicit solutions to (11) for the SPP wavenumber in terms of the propagation angle exist and can be written in the form

$$q^{\pm} = k\sqrt{R^{\pm} + iI^{\pm}}, \tag{12}$$

where $k = \omega\sqrt{\varepsilon\mu}$, $R^{\pm}$ and $I^{\pm}$ denote the real and imaginary parts of the argument of the square root respectively, and the $\pm$ distinguishes between the two solutions corresponding to QTE and QTM SPP modes. The usual branch of the square root is assumed in which $\mathrm{Re}(q^{\pm}) > 0$. It is important to note that $\mathrm{sgn}\left(\mathrm{Im}\left\{q^{\pm}\right\}\right)$ is equal to that of $I^{\pm}$. It can be shown that

$$R^{\pm} = 1 + \frac{2\left|\Delta^{\pm}\right|}{\eta^2\left|\sigma_{\hat{\mathbf{q}}\hat{\mathbf{q}}}\right|^2}\cos\left(2\theta + \gamma^{\pm}\right), \tag{13}$$
$$I^{\pm} = \frac{2\left|\Delta^{\pm}\right|}{\eta^2\left|\sigma_{\hat{\mathbf{q}}\hat{\mathbf{q}}}\right|^2}\sin\left(2\theta + \gamma^{\pm}\right), \tag{14}$$

where

$$\Delta^{\pm} = s^4 - 2s_d^2 \mp s^2\sqrt{s^4 - 4s_d^2}, \tag{15}$$

with $s^2 = 1 + \eta^2\det(\bar{\sigma})/4$, $s_d^2 = \eta^2\sigma_{\hat{\mathbf{q}}\hat{\mathbf{q}}}\sigma_{(\hat{\mathbf{z}}\times\hat{\mathbf{q}})(\hat{\mathbf{z}}\times\hat{\mathbf{q}})}/4$, and $\eta^2 = \mu/\varepsilon$. The angles $\theta, \gamma^{\pm} \in [-\pi, \pi]$ are defined as

$$\theta = \mathrm{sgn}\left(\mathrm{Im}\left\{\sigma_{\hat{\mathbf{q}}\hat{\mathbf{q}}}\right\}\right)\tan^{-1}\left(\frac{\mathrm{Re}\left\{\sigma_{\hat{\mathbf{q}}\hat{\mathbf{q}}}\right\}}{\left|\mathrm{Im}\left\{\sigma_{\hat{\mathbf{q}}\hat{\mathbf{q}}}\right\}\right|}\right), \tag{16}$$
$$\gamma^{\pm} = \tan^{-1}\left(\frac{\mathrm{Im}\left\{\Delta^{\pm}\right\}}{\mathrm{Re}\left\{\Delta^{\pm}\right\}}\right). \tag{17}$$

Assuming low loss, the conductivity elements in the standard basis are of the form $\sigma_{\alpha\alpha} = i\mathrm{Im}\{\sigma_{\alpha\alpha}\} + \varepsilon_{\alpha\alpha}$ and $\sigma_{\alpha\beta} = \mathrm{Re}\left\{\sigma_{\alpha\beta}\right\} + i\varepsilon_{\alpha\beta}$ for $\alpha, \beta \in \{\hat{\mathbf{x}}, \hat{\mathbf{y}}\}$ ($\alpha \neq \beta$) such that $|\mathrm{Im}(\sigma_{\alpha\alpha})| \gg |\varepsilon_{\alpha\alpha}|$ and $\left|\mathrm{Re}\left(\sigma_{\alpha\beta}\right)\right| \gg \left|\varepsilon_{\alpha\beta}\right|$. Both $\varepsilon_{\alpha\alpha}$ and $\varepsilon_{\alpha\beta}$ are real valued with $\varepsilon_{\alpha\alpha} > 0$ while the sign of $\varepsilon_{\alpha\beta}$ is determined with respect to an arbitrary axis along which time reversal symmetry is broken. In this case, we find $0 < \mathrm{Re}\left\{\sigma_{\hat{\mathbf{q}}\hat{\mathbf{q}}}\right\} \ll \left|\mathrm{Im}\left\{\sigma_{\hat{\mathbf{q}}\hat{\mathbf{q}}}\right\}\right|$, and therefore, the sign of $\mathrm{Im}\left\{\sigma_{\hat{\mathbf{q}}\hat{\mathbf{q}}}\right\}$ ultimately determines whether θ is in the first $[0, \pi/2]$ or fourth $[-\pi/2, 0]$ quadrants of the complex plane.

In most cases, QTE SPP modes are fast propagating with small wavenumber (i.e., $q^+ \simeq k$). As a result, these modes tend to leak rapidly into the surrounding environment and are loosely confined to the interface. Therefore, these modes are of little importance and are not considered in the following analysis. In contrast, QTM modes tend to be slow propagating with large wavenumber (i.e., $q^- \gtrsim k$) and tightly confined to the interface[39] which is ideal. It is straightforward to show, in the isotropic case, that

$$\left|\frac{\mathrm{Im}\left\{\Delta^-\right\}}{\mathrm{Re}\left\{\Delta^-\right\}}\right| < \left|\frac{\mathrm{Re}\left\{\sigma_{\hat{\mathbf{q}}\hat{\mathbf{q}}}\right\}}{\mathrm{Im}\left\{\sigma_{\hat{\mathbf{q}}\hat{\mathbf{q}}}\right\}}\right|, \tag{18}$$

and although difficult to formally prove, it is reasonable to assume (18) also holds in the anisotropic case, as numerical tests have confirmed. We then find

$$\left|\gamma^-\right| = \tan^{-1}\left|\frac{\mathrm{Im}\{\Delta^-\}}{\mathrm{Re}\{\Delta^-\}}\right| < \tan^{-1}\left|\frac{\mathrm{Re}\{\sigma_{\hat{\mathbf{q}}\hat{\mathbf{q}}}\}}{\mathrm{Im}\{\sigma_{\hat{\mathbf{q}}\hat{\mathbf{q}}}\}}\right| = |\theta|, \quad (19)$$

indicating that $2\theta+\gamma^-$ and 2θ share the same quadrant. As a result, one is justified in writing (14) in the form

$$I^- = \mathrm{sgn}\left(\mathrm{Im}\{\sigma_{\hat{\mathbf{q}}\hat{\mathbf{q}}}\}\right)\left[\frac{2|\Delta^-|}{\eta^2\left|\sigma_{\hat{\mathbf{q}}\hat{\mathbf{q}}}\right|^2}\sin\left|2\theta+\gamma^-\right|\right], \quad (20)$$

where the term in brackets $[\cdot]$ is positive, making it clear that $\mathrm{sgn}\left(\mathrm{Im}\{\sigma_{\hat{\mathbf{q}}\hat{\mathbf{q}}}\}\right)$ controls the sign of I^- and ultimately $\mathrm{Im}\{q^-\}$.

Outward propagating QTM SPP modes along a particular direction in the plane of the interface are required to have $\mathrm{Im}\{q\} > 0$ in order to satisfy the Sommerfeld radiation condition. This condition is satisfied when $I^- > 0$ and therefore, $\mathrm{Im}\{\sigma_{\hat{\mathbf{q}}\hat{\mathbf{q}}}\} > 0$. We characterize the conductivity as inductive according to $\mathrm{Im}\{\sigma_{\hat{\mathbf{q}}\hat{\mathbf{q}}}\} > 0$, which remains valid in the isotropic limit.

To summarize, we find that local dispersive, anisotropic two-dimensional materials, support QTM SPP modes when the effective conductivity seen by the wave along the propagation direction $\sigma_{\hat{\mathbf{q}}\hat{\mathbf{q}}}(\omega,\phi)$ defined in (5) is inductive, with a positive imaginary part. In the limiting cases $\phi = 2n\pi$ and $\phi = n\pi+\pi/2$ for $n \in \{0,1,2,\dots\}$, we find $\sigma_{\hat{\mathbf{q}}\hat{\mathbf{q}}} = \sigma_{\hat{\mathbf{x}}\hat{\mathbf{x}}}, \sigma_{\hat{\mathbf{y}}\hat{\mathbf{y}}}$ respectively; the other diagonal element is effectively immaterial in these limits. As a result, predicting the spectral location of bandgaps in the QTM SPP dispersion is straightforward.

Lastly, we note that in most cases, natural 2d/quasi-2D materials are supported by a substrate of some kind. In this case, the closed form solutions to the dispersion relation (11) obtained and the above analysis no-longer rigorously applies as the material properties above and below the material would differ. However, as long as the substrate plays a negligible role in guiding the SPP, the above analysis is still useful.

III. RESULTS AND DISCUSSION

Here, we present two examples to validate the presented formulation. We consider excitation frequencies up into the infrared region of the spectrum, and take the surrounding medium to be vacuum.

A. Gyrotropic Graphene

In this example, we consider graphene biased with a perpendicular external magnetic field $\mathbf{B} = \hat{\mathbf{z}}B_0$ [T]. The conductivity tensor in the standard basis is of the form (1) with $\sigma_{\hat{\mathbf{x}}\hat{\mathbf{x}}} = \sigma_{\hat{\mathbf{y}}\hat{\mathbf{y}}} = \sigma_d$ and $\sigma_{\hat{\mathbf{x}}\hat{\mathbf{y}}} = -\sigma_{\hat{\mathbf{y}}\hat{\mathbf{x}}} = \sigma_o$ where $\sigma_{d,o} = \sigma_{d,o}^{\mathrm{intra}} + \sigma_{d,o}^{\mathrm{inter}}$, with intra- and inter- band contributions written as a discrete summation over Landau levels[40]

$$\sigma_d^{\mathrm{inter/intra}} = \frac{\hbar\tilde{\omega}}{i}\frac{e^2E_1^2}{2\pi\hbar}\sum_{n=0}^{\infty}\frac{1}{M_n^\pm}\frac{N_{n+1}^- \pm N_n^-}{M_n^\pm M_n^\pm - \hbar^2\tilde{\omega}^2}, \quad (21)$$

$$\sigma_o^{\mathrm{inter/intra}} = \mathrm{sgn}(B_0)\frac{e^2E_1^2}{2\pi\hbar}\sum_{n=0}^{\infty}\frac{N_{n+1}^+ - N_n^+}{M_n^\pm M_n^\pm - \hbar^2\tilde{\omega}^2}, \quad (22)$$

where $N_n^\pm = n_F(-E_n) \pm n_F(E_n)$ and $M_n^\pm = E_{n+1} \pm E_n$ with $\tilde{\omega} = \omega + 2i\Gamma$, $E_n = v_F\sqrt{2\hbar n|eB_0|}$, and $n_F(E) = \{\exp[(E-\mu_c)/k_BT]+1\}^{-1}$ is the Fermi-Dirac distribution function. The parameters $\{\omega,\Gamma,\mu_c,v_F,e,T,\hbar,k_B\}$ denote the excitation frequency, scattering rate, chemical potential, Fermi velocity $\simeq 10^6\mathrm{m/s}$, fundamental charge, temperature, Planck's reduced constant, and Boltzmann constant respectively. One additional parameter worth introducing is the magnetic length $l_B = \sqrt{\hbar/|eB_0|}$. This quantity places a bound on q in the sense that for $q \gtrsim 1/l_B$ a non-local model for the conductivity is required[33]. It should also be noted that for relatively large magnetic field values ($B_0 \gtrsim 0.1T$), the infinite sums in (21)-(22) converge rather quickly, making it sufficient to include only a few terms. This yields the correct result for frequencies up to the first few landau levels, however, additional terms are necessary at higher frequencies to obtain the correct resonance behavior.

The QTM dispersion and associated equi-frequency dispersion contours are shown in Figs. 2a and 2b respectively, while the imaginary part of $\sigma_{\hat{\mathbf{q}}\hat{\mathbf{q}}}$ is shown in Fig. 2c. Isotropy in the diagonal elements results in isotropic equi-frequency contours as the dependence on ϕ drops out of $\sigma_{\hat{\mathbf{q}}\hat{\mathbf{q}}}$. Bandgaps in the exact dispersion (12) clearly correspond to $\mathrm{Im}\{\sigma_{\hat{\mathbf{q}}\hat{\mathbf{q}}}\} < 0$, indicated by the blue shaded regions.

B. Hyperbolic, Black Phosphorous

Next, we consider an approximate model for the conductivity of multilayer black phosphorous thin films[11,12] where anisotropy arises as a consequence of the in-plane crystallographic directions having different symmetries. In the hyperbolic regime, the imaginary parts of $\sigma_{\hat{\mathbf{x}}\hat{\mathbf{x}}}$ and $\sigma_{\hat{\mathbf{y}}\hat{\mathbf{y}}}$ are of opposite sign, in which case the the sign of the imaginary part of $\sigma_{\hat{\mathbf{q}}\hat{\mathbf{q}}}$ may vary depending on propagation angle and excitation frequency. In what follows, we restrict our consideration to bandgap dependence on propagation angle.

At sufficiently low frequency, intraband transitions dominate the material response and lead to a Drude type contribution to the conductivity of the form $\sigma_{\alpha\alpha}^{\mathrm{intra}} = i\Omega_{\alpha\alpha}/\tilde{\omega}$ for $\alpha \in \{\hat{\mathbf{x}},\hat{\mathbf{y}}\}$, where $\tilde{\omega} = \omega + 2i\Gamma$ and $\Omega_{\alpha\alpha} = e^2|n|/m_\alpha^*$ denotes the drude weight. The parameters $\{\omega,\Gamma,n,m_\alpha^*,e\}$ denote the excitation frequency, scattering rate, charge carrier density, fundamental charge, and effective mass respectively. At higher frequencies, inter-band transitions dominate. However, in the case of multilayer black phosphorous, the interband transitions are negligible along one of the crystallographic directions which we conveniently take to be $\hat{\mathbf{y}}$. Thus, $\sigma_{\hat{\mathbf{y}}\hat{\mathbf{y}}}$ has only an intraband contribution while $\sigma_{\hat{\mathbf{x}}\hat{\mathbf{x}}}$ has both intra- and inter-band contributions. We introduce the interband contribution phonologically by modeling the absorption

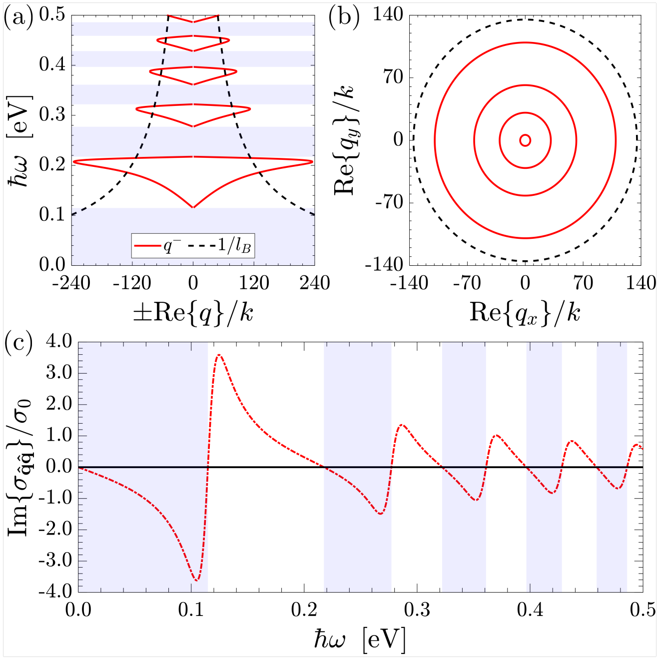

FIG. 2. (a) QTM SPP dispersion (red lines) with bandgaps shaded purple and (b) isotropic equi-frequency dispersion contours increasing in radius for the respective energies $\{0.12\text{eV}, 0.14\text{eV}, 0.16\text{eV}, 0.18\text{eV}\}$. (c) Behavior of $\mathrm{Im}\{\sigma_{\hat{q}\hat{q}}\}$ shows how spectral regions in which the sign is negative correspond to the bandgap regions in (a). Material parameters used in the conductivity model are $\hbar\Gamma = 0.005$eV, $\mu_c = 0.3E_1 \simeq 0.03$eV, $B_0 = 10$T, and $T = 40$K.

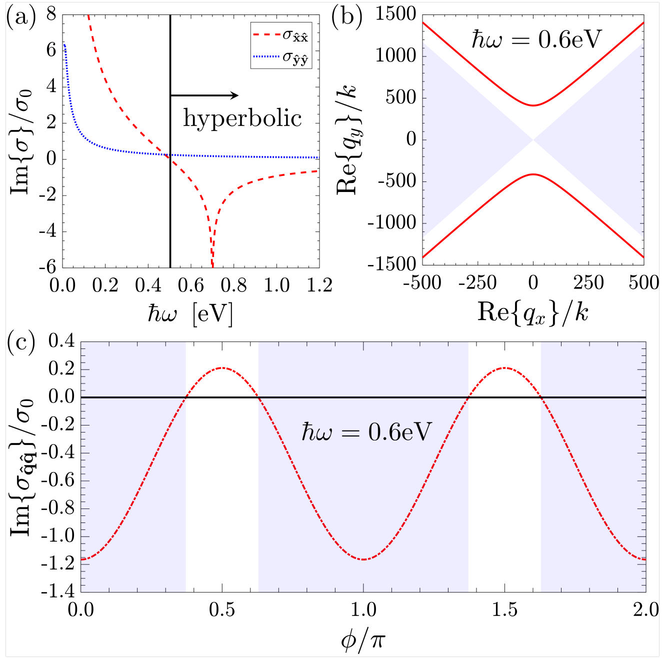

FIG. 3. (a) Conductivity tensor elements represented in the standard basis for a Black Phosphorous film. The hyperbolic regime in which $\mathrm{Im}\{\sigma_{\hat{x}\hat{x}}\}\mathrm{Im}\{\sigma_{\hat{y}\hat{y}}\} < 0$ is located to the right of the vertical black line. (b) The hyperbolic equi-frequency dispersion contour for $\hbar\omega = 0.2$eV. Bandgaps in the equi-frequency contours (shaded blue) are determined by $\mathrm{Im}\{\sigma_{\hat{q}\hat{q}}\} < 0$ shown in (c). Material parameters used in the conductivity model are $\hbar\Gamma = 0.005$eV, $n = 5\text{e}13\text{cm}^{-2}$, $m^*_{\hat{x}} = 0.15m_0$, $m^*_{\hat{y}} = 1.2m_0$, $\hbar\omega_{\hat{x}} = 0.7$eV, and $\sigma_{\hat{x}} = 3.5\sigma_0$ where m_0 denotes the free electron rest mass and $\sigma_0 = e^2/4\hbar$.

(real part) as a unit step and obtain the imaginary part from the Kramers-Kronig relations. In total, we have[41]

$$\sigma^{\text{inter}}_{\hat{x}\hat{x}} = \sigma_{\hat{x}}\left[\Theta(\omega - \omega_{\hat{x}}) + \frac{i}{\pi}\ln\left|\frac{\omega - \omega_{\hat{x}}}{\omega + \omega_{\hat{x}}}\right|\right], \qquad (23)$$

where $\omega_{\hat{x}}$ denotes the onset frequency of inter-band transitions and $\sigma_{\hat{x}}$ is an amplitude coefficient.

Figure 3a shows how the imaginary parts of the conductivity elements in the standard basis vary with respect to frequency. The solid black vertical line separates the elliptic and hyperbolic regimes. Parameters used in the conductivity model correspond to a 20nm thick Black Phosphorus film[12], doped with a 0.2eV chemical potential defined as the energy difference between Fermi level and first conduction subband. For $\hbar\omega = 0.6$eV, the equi-frequency dispersion contour (EFC) is shown in Fig. 3b, and the imaginary part of $\sigma_{\hat{q}\hat{q}}$ as propagation angle varies is shown in Fig. 3c. Bandgaps in the EFC are shaded blue and agree with $\mathrm{Im}\{\sigma_{\hat{q}\hat{q}}\} < 0$.

IV. CONCLUSION

In this work, we used the conductivity of local, dispersive, anisotropic two-dimensional materials to predict the spectral location of bandgaps in the QTM SPP dispersion. These bandgaps are found to occur in regions of the spectrum where the imaginary part of the conductivity along the direction of propagation is negative (i.e., $\mathrm{Im}\{\sigma_{\hat{q}\hat{q}}\} < 0$) which remains valid in the isotropic limit. Conversely, we found that QTM SPP mode propagation is supported by inductive surfaces, which we characterized according to $\mathrm{Im}\{\sigma_{\hat{q}\hat{q}}\} > 0$. To demonstrate our proposed formalism, we provided two numerical examples of natural materials. We believe these results to be extremely helpful in the characterization of natural 2D/quasi-2D materials, and in artificial metasurface design.

ACKNOWLEDGMENTS

Funding for this research was provided by the National Science Foundation under grant number EFMA-1741673.

DATA AVAILABILITY

The data that support the findings of this study are available from the corresponding author upon reasonable request.

Appendix A: SPP Dispersion Relation

In the following, we obtain the natural modes of the 2D/quasi-2D structure shown in Fig. 1. These modes are defined as a field configuration that exists in the absence of sources and satisfies the appropriate boundary conditions.

Above and below the interface, in the isotropic dielectric regions, Maxwell's equations in the absence of sources combine to form the wave equation for the electric and magnetic fields (i.e., the vector Helmholtz equation)

$$\nabla^2\mathbf{\Psi}+\omega^2\mu\varepsilon\mathbf{\Psi}=\nabla\nabla\cdot\mathbf{\Psi} \tag{A1}$$

for $\mathbf{\Psi}\in\{\mathbf{E},\mathbf{H}\}$ where $\nabla\cdot\mathbf{\Psi}=\mathbf{0}$. The general solutions to (A1) in spacial transform domain with respect to x,y are $\mathbf{\Psi}^m(\mathbf{q},z)=\mathbf{\Psi}_0^m(\mathbf{q})\exp\left(ik_z^m z\right)$, where $\mathbf{q}=\hat{\mathbf{x}}q_x+\hat{\mathbf{y}}q_y$ is the in-plane wavevector preserved across the interface, $\mathbf{\Psi}_0^m\in\left\{\mathbf{E}_0^m,\mathbf{H}_0^m\right\}$ is the polarization, and $k_z^m=m\sqrt{k^2-q^2}$ with $k^2=\omega^2\mu\varepsilon$ and $m\in\{\pm\}$ used to indicate forward/backward propagation with respect to the z-direction.

Expanding $\mathbf{E}_0^m$ in a coordinate system spanned by the unit vectors $\{\hat{\mathbf{z}},\hat{\mathbf{q}},\hat{\mathbf{z}}\times\hat{\mathbf{q}}\}$, we have

$$\mathbf{E}_0^m=E_{\hat{\mathbf{q}}}^m\hat{\mathbf{q}}+E_{\hat{\mathbf{z}}}^m\hat{\mathbf{z}}+E_{\hat{\mathbf{z}}\times\hat{\mathbf{q}}}^m\left(\hat{\mathbf{z}}\times\hat{\mathbf{q}}\right), \tag{A2}$$

and choosing the tangential components $E_{\hat{\mathbf{q}}}^m$ and $E_{\hat{\mathbf{z}}\times\hat{\mathbf{q}}}^m$, it follows that $E_{\hat{\mathbf{z}}}^m=-qE_{\hat{\mathbf{q}}}^m/k_z^m$. The associated magnetic field polarization is obtained from Faraday's law as

$$\omega\mu\mathbf{H}_0^m=-k_z^mE_{\hat{\mathbf{z}}\times\hat{\mathbf{q}}}^m\hat{\mathbf{q}}+\frac{k^2}{k_z^m}E_{\hat{\mathbf{q}}}^m\left(\hat{\mathbf{z}}\times\hat{\mathbf{q}}\right)+qE_{\hat{\mathbf{z}}\times\hat{\mathbf{q}}}^m\hat{\mathbf{z}}. \tag{A3}$$

From (A2) and (A3), it is straightforward to recover the relation $\hat{\mathbf{z}}\times\mathbf{H}_{0\|}^m=m\bar{\mathbf{Y}}\cdot\mathbf{E}_{0\|}^m$, where $\mathbf{E}_{0\|}^m,\mathbf{H}_{0\|}^m$ are the tangential components of the polarization and

$$\bar{\mathbf{Y}}=\frac{-1}{\omega\mu\sqrt{k^2-q^2}}\begin{pmatrix}k^2 & 0\\ 0 & k^2-q^2\end{pmatrix}. \tag{A4}$$

Applying the typical outgoing wave conditions in the unbounded regions (i.e., $z\to\pm\infty$) and enforcing the boundary conditions at the interface (9)-(10) leads to

$$\left(2\bar{\mathbf{Y}}-\bar{\boldsymbol{\sigma}}\right)\cdot\mathbf{E}_{0\|}^+=\mathbf{0}, \tag{A5}$$

for which non-trivial solutions are obtained when

$$\det\left(2\bar{\mathbf{Y}}-\bar{\boldsymbol{\sigma}}\right)=0. \tag{A6}$$

Valid solutions to (A6) take the form of ω,q pairs which describe the natural, propagating SPP modes supported by the structure.

[1] J. Zhang, L. Zhang, and W. Xu, "Surface plasmon polaritons: physics and applications," Journal of Physics D: Applied Physics **45**, 113001 (2012).
[2] K. S. Novoselov, A. K. Geim, S. V. Morozov, D. Jiang, Y. Zhang, S. V. Dubonos, I. V. Grigorieva, and A. A. Firsov, "Electric field effect in atomically thin carbon films," Science **306**, 666–669 (2004).
[3] K. Novoselov, A. Geim, S. Morozov, D. Jiang, M. Katsnelson, I. Grigorieva, S. Dubonos, and A. Firsov, "Two-dimensional gas of massless dirac fermions in graphene," Nature **438**, 197–200 (2005).
[4] Q. Wang, K. Kalantar-Zadeh, A. Kis, J. Coleman, and M. Strano, "Electronics and optoelectronics of two-dimensional transition metal dichalcogenides," Nature Nanotechnology **7**, 699–712 (2012).
[5] M. Osada and T. Sasaki, "Two-dimensional dielectric nanosheets: Novel nanoelectronics from nanocrystal building blocks," Advanced Materials **24**, 210–228 (2012).
[6] A. Ayari, E. Cobas, O. Ogundadegbe, and M. S. Fuhrer, "Realization and electrical characterization of ultrathin crystals of layered transition-metal dichalcogenides," Journal of Applied Physics **101**, 014507 (2007).
[7] Z. Jacob, "Nanophotonics: Hyperbolic phonon-polaritons," Nature materials **13**, 1081–3 (2014).
[8] W. Qu, F. Gou, and C. Ke, "Thermal-induced irreversible straining of ultrathin boron nitride nanosheets," Applied Physics Letters **114**, 051901 (2019).
[9] D. Pacilé, J. C. Meyer, Girit, and A. Zettl, "The two-dimensional phase of boron nitride: Few-atomic-layer sheets and suspended membranes," Applied Physics Letters **92**, 133107 (2008).
[10] H. Hajian, I. D. Rukhlenko, G. W. Hanson, T. Low, B. Butun, and E. Ozbay, "Tunable plasmon-phonon polaritons in anisotropic 2d materials on hexagonal boron nitride," Nanophotonics , 20200080 (2020).
[11] T. Low, R. Roldán, H. Wang, F. Xia, P. Avouris, L. M. Moreno, and F. Guinea, "Plasmons and screening in monolayer and multilayer black phosphorus," Phys. Rev. Lett. **113**, 106802 (2014).
[12] T. Low, A. S. Rodin, A. Carvalho, Y. Jiang, H. Wang, F. Xia, and A. H. Castro Neto, "Tunable optical properties of multilayer black phosphorus thin films," Phys. Rev. B **90**, 075434 (2014).
[13] A. Carvalho, M. Wang, X. Zhu, A. Rodin, H. Su, and A. Castro Neto, "Phosphorene: From theory to applications," Nature Reviews Materials **1**, 16061 (2016).
[14] M. Sherrott, W. Whitney, D. Jariwala, S. Biswas, C. Went, J. Wong, G. Rossman, and H. Atwater, "Anisotropic quantum well electro-optics in few-layer black phosphorus," Nano Letters **19** (2018), 10.1021/acs.nanolett.8b03876.
[15] Z. Liu and K. Aydin, "Localized surface plasmons in nanostructured monolayer black phosphorus," Nano letters **16** (2016), 10.1021/acs.nanolett.5b05166.
[16] S. A. Dereshgi, Z. Liu, and K. Aydin, "Anisotropic localized surface plasmons in borophene," Opt. Express **28**, 16725–16739.
[17] G. Álvarez Pérez, T. G. Folland, I. Errea, J. Taboada-Gutiérrez, J. Duan, J. Martín-Sánchez, A. I. F. Tresguerres-Mata, J. R. Matson, A. Bylinkin, M. He, W. Ma, Q. Bao, J. I. Martín, J. D. Caldwell, A. Y. Nikitin, and P. Alonso-González, "Infrared permittivity of the biaxial van der waals semiconductor α-moo3 from near- and far-field correlative studies," Advanced Materials **32**, 1908176 (2020).
[18] A. Geim and I. Grigorieva, "Van der waals heterostructures," Nature **499**, 419–25 (2013).
[19] L. Ponomarenko, A. Geim, A. Zhukov, R. Jalil, S. Morozov, K. Novoselov, V. Cheianov, V. Falko, K. Watanabe, T. Taniguchi, and R. Gorbachev, "Tunable metal-insulator transition in double-layer graphene heterostructures," Nature Physics **7** (2011), 10.1038/nphys2114.
[20] L. Britnell, R. Gorbachev, R. Jalil, B. Belle, F. Schedin, A. Mishchenko, T. Georgiou, M. Katsnelson, L. Eaves, S. Morozov, N. Peres, J. Leist, A. Geim, K. Novoselov, and L. Ponomarenko, "Field-effect tunneling transistor based on vertical graphene heterostructures," Science (New York, N.Y.) **335**, 947–50 (2012).
[21] T. Georgiou, R. Jalil, B. Belle, L. Britnell, R. Gorbachev, S. Morozov, Y.-J. Kim, A. Gholinia, S. Haigh, O. Makarovsky, L. Eaves, L. Ponomarenko, A. Geim, K. Novoselov, and A. Mishchenko, "Vertical field-effect transistor based on graphene-ws 2 heterostructures for flexible and transparent electronics," Nature nanotechnology **8** (2012), 10.1038/nnano.2012.224.
[22] S. Inampudi, M. Nazari, A. Forouzmand, and H. Mosallaei, "Manipulation of surface plasmon polariton propagation on isotropic and anisotropic two-dimensional materials coupled to boron nitride heterostructures," Journal of Applied Physics **119**, 025301 (2016).
[23] A. M. Holmes, S. Pakniyat, S. A. H. Gangaraj, F. Monticone, M. Weinert, and G. W. Hanson, "Exchange splitting and exchange-induced nonreciprocal photonic behavior of graphene in Cri_3-graphene van der waals heterostructures," Phys. Rev. B **102**, 075435 (2020).
[24] K. Novoselov, A. Mishchenko, A. Carvalho, and A. Castro Neto, "2d materials and van der waals heterostructures," Science **353**, aac9439–aac9439

(2016).

[25] V. Lenets, O. Yermakov, A. Sayanskiy, J. Baena, E. Martini, S. Glybovski, and S. Maci, "Surface waves on self-complementary metasurfaces: intrinsic hyperbolicity, dual-directional canalization and te-tm polarization degeneracy," (2020), arXiv:2004.06038 [physics.app-ph].

[26] N. yu and F. Capasso, "Flat optics with designer metasurfaces," Nature materials **13**, 139–50 (2014).

[27] A. Kildishev, A. Boltasseva, and V. Shalaev, "Planar photonics with metasurfaces," Science (New York, N.Y.) **339**, 1232009 (2013).

[28] T. Badloe, J. Mun, and J. Rho, "Metasurfaces-based absorption and reflection control: Perfect absorbers and reflectors," Journal of Nanomaterials **2017**, 1–18 (2017).

[29] J. Gomez-Diaz, M. Tymchenko, and A. Alù, "Hyperbolic metasurfaces: Surface plasmons, light-matter interactions, and physical implementation using graphene strips," Optical Materials Express **5**, 2313 (2015).

[30] K. Khaliji, A. Fallahi, L. Martin-Moreno, and T. Low, "Tunable plasmon-enhanced birefringence in ribbon array of anisotropic two-dimensional materials," Physical Review B **95**, 201401 (2017).

[31] D. Jin, T. Christensen, M. Soljačić, N. Fang, L. Lu, and X. Zhang, "Infrared topological plasmons in graphene," Physical Review Letters **118** (2017), 10.1103/PhysRevLett.118.245301.

[32] A. Kumar, A. Nemilentsau, K. H. Fung, G. Hanson, N. Fang, and T. Low, "Chiral plasmon in gapped dirac systems," Physical Review B **93**, 041413(R) (2016).

[33] A. Ferreira, N. Peres, and A. Castro Neto, "Confined magneto-optical waves in graphene," Physical Review B **85** (2012), 10.1103/PhysRevB.85.205426.

[34] G. Hanson, "Dyadic green's functions for an anisotropic, non-local model of biased graphene," Antennas and Propagation, IEEE Transactions on **56**, 747 – 757 (2008).

[35] j.-m. Poumirol, P. Liu, T. Slipchenko, A. Nikitin, L. Martin-Moreno, J. Faist, and A. Kuzmenko, "Electrically controlled terahertz magneto-optical phenomena in continuous and patterned graphene," Nature Communications **8** (2017), 10.1038/ncomms14626.

[36] S. Pakniyat, A. M. Holmes, G. W. Hanson, S. A. H. Gangaraj, M. Antezza, M. G. Silveirinha, S. Jam, and F. Monticone, "Non-reciprocal, robust surface plasmon polaritons on gyrotropic interfaces," IEEE Transactions on Antennas and Propagation **68**, 3718–3729 (2020).

[37] S. A. Hassani Gangaraj, T. Low, A. Nemilentsau, and G. W. Hanson, "Directive surface plasmons on tunable two-dimensional hyperbolic metasurfaces and black phosphorus: Green's function and complex plane analysis," IEEE Transactions on Antennas and Propagation **65**, 1174–1186 (2017).

[38] X.-Y. He, "Comparison of graphene-based transverse magnetic and electric surface plasmon modes," IEEE Journal of Selected Topics in Quantum Electronics **20**, 4600106 (2014).

[39] G. W. Hanson, "Dyadic green's functions and guided surface waves for a surface conductivity model of graphene," Journal of Applied Physics **103**, 064302 (2008).

[40] V. Gusynin, S. Sharapov, and J. Carbotte, "Magneto-optical conductivity in graphene," Journal of Physics: Condensed Matter **19** (2007), 10.1088/0953-8984/19/2/026222.

[41] A. Nemilentsau, T. Low, and G. Hanson, "Anisotropic 2d materials for tunable hyperbolic plasmonics," Phys. Rev. Lett. **116**, 066804 (2016).

[42] L. A. Falkovsky, "Optical properties of graphene," Journal of Physics: Conference Series **129**, 012004 (2008).

[43] V. P. Gusynin, S. G. Sharapov, and J. P. Carbotte, "Sum rules for the optical and hall conductivity in graphene," Phys. Rev. B **75**, 165407 (2007).

[44] P. R. Wallace, "The band theory of graphite," Phys. Rev. **71**, 622–634 (1947).

[45] F. Liang, G. W. Hanson, A. B. Yakovlev, G. Lovat, P. Burghignoli, R. Araneo, and S. A. Hassani Gangaraj, "Dyadic green's functions for dipole excitation of homogenized metasurfaces," IEEE Transactions on Antennas and Propagation **64**, 167–178 (2016).

[46] S. Paulotto, P. Baccarelli, P. Burghignoli, G. Lovat, G. W. Hanson, and A. B. Yakovlev, "Homogenized green's functions for an aperiodic line source over planar densely periodic artificial impedance surfaces," IEEE Transactions on Microwave Theory and Techniques **58**, 1807–1817 (2010).

[47] P. Pons-Valencia, F. Alfaro-Mozaz, M. Wiecha, V. Biolek, I. Dolado, S. Vélez, P. Li, P. Alonso-González, F. Casanova, L. Hueso, L. Martín-Moreno, R. Hillenbrand, and A. Nikitin, "Launching of hyperbolic phonon-polaritons in h-bn slabs by resonant metal plasmonic antennas," Nature Communications **10** (2019), 10.1038/s41467-019-11143-7.

[48] Y. Zhou, G. Scuri, D. Wild, A. High, A. Dibos, L. Jauregui, C. Shu, K. De Greve, K. Pistunova, A. Joe, T. Taniguchi, K. Watanabe, P. Kim, M. Lukin, and H. Park, "Probing dark excitons in atomically thin semiconductors via near-field coupling to surface plasmon polaritons," Nature nanotechnology **12** (2017), 10.1038/nnano.2017.106.

[49] P. A. D. Gonçalves, S. Xiao, N. M. R. Peres, and N. A. Mortensen, "Hybridized plasmons in 2d nanoslits: From graphene to anisotropic 2d materials," ACS Photonics **4**, 3045–3054 (2017), https://doi.org/10.1021/acsphotonics.7b00558.

[50] C. Liu, H. Chen, S. Wang, Q. Liu, Y.-G. Jiang, D. Zhang, M. Liu, and P. Zhou, "Two-dimensional materials for next-generation computing technologies," Nature Nanotechnology **15**, 545–557 (2020).

[51] Y. Li and T. F. Heinz, "Two-dimensional models for the optical response of thin films," 2D Materials **5**, 025021 (2018).

[52] G. W. Hanson, "Dyadic green's functions and guided surface waves for a surface conductivity model of graphene," Journal of Applied Physics **103**, 064302 (2008), https://doi.org/10.1063/1.2891452.

[53] F. Monticone and A. Alù, "Metamaterial, plasmonic and nanophotonic devices," Reports on Progress in Physics **80**, 036401 (2017).

[54] P. Li, I. Dolado, F. J. Alfaro-Mozaz, A. Y. Nikitin, F. Casanova, L. E. Hueso, S. Vélez, and R. Hillenbrand, "Optical nanoimaging of hyperbolic surface polaritons at the edges of van der waals materials," Nano Letters **17**, 228–235 (2017), pMID: 27966994, https://doi.org/10.1021/acs.nanolett.6b03920.

[55] A. Dubrovkin, B. Qiang, T. Salim, D. Nam, N. Zheludev, and Q. Wang, "Resonant nanostructures for highly confined and ultra-sensitive surface phonon-polaritons," Nature Communications **11** (2020), 10.1038/s41467-020-15767-y.

[56] H. Hajian, I. D. Rukhlenko, G. W. Hanson, T. Low, B. Butun, and E. Ozbay, "Tunable plasmon-phonon polaritons in anisotropic 2d materials on hexagonal boron nitride," Nanophotonics , 20200080 (2020).

[57] A. Hassani Gangaraj, G. Hanson, M. Silveirinha, K. Shastri, M. Antezza, and F. Monticone, "Unidirectional and diffractionless surface plasmon polaritons on three-dimensional nonreciprocal plasmonic platforms," Physical Review B **99** (2019), 10.1103/PhysRevB.99.245414.

[58] G. Hanson, A. Hassani Gangaraj, and A. Nemilentsau, "Unidirectional, defect-immune, and topologically protected electromagnetic surface waves," (2018) pp. 569–604.

[59] M. Fox, *Quantum optics: an introduction*, Oxford master series in atomic, optical, and laser physics (Oxford Univ. Press, Oxford, 2006).

[60] J. Bernard, L. Fleury, H. Talon, and M. Orrit, "Photon bunching in the fluorescence from single molecules: A probe for intersystem crossing," The Journal of Chemical Physics **98**, 850–859 (1993), https://doi.org/10.1063/1.464249.

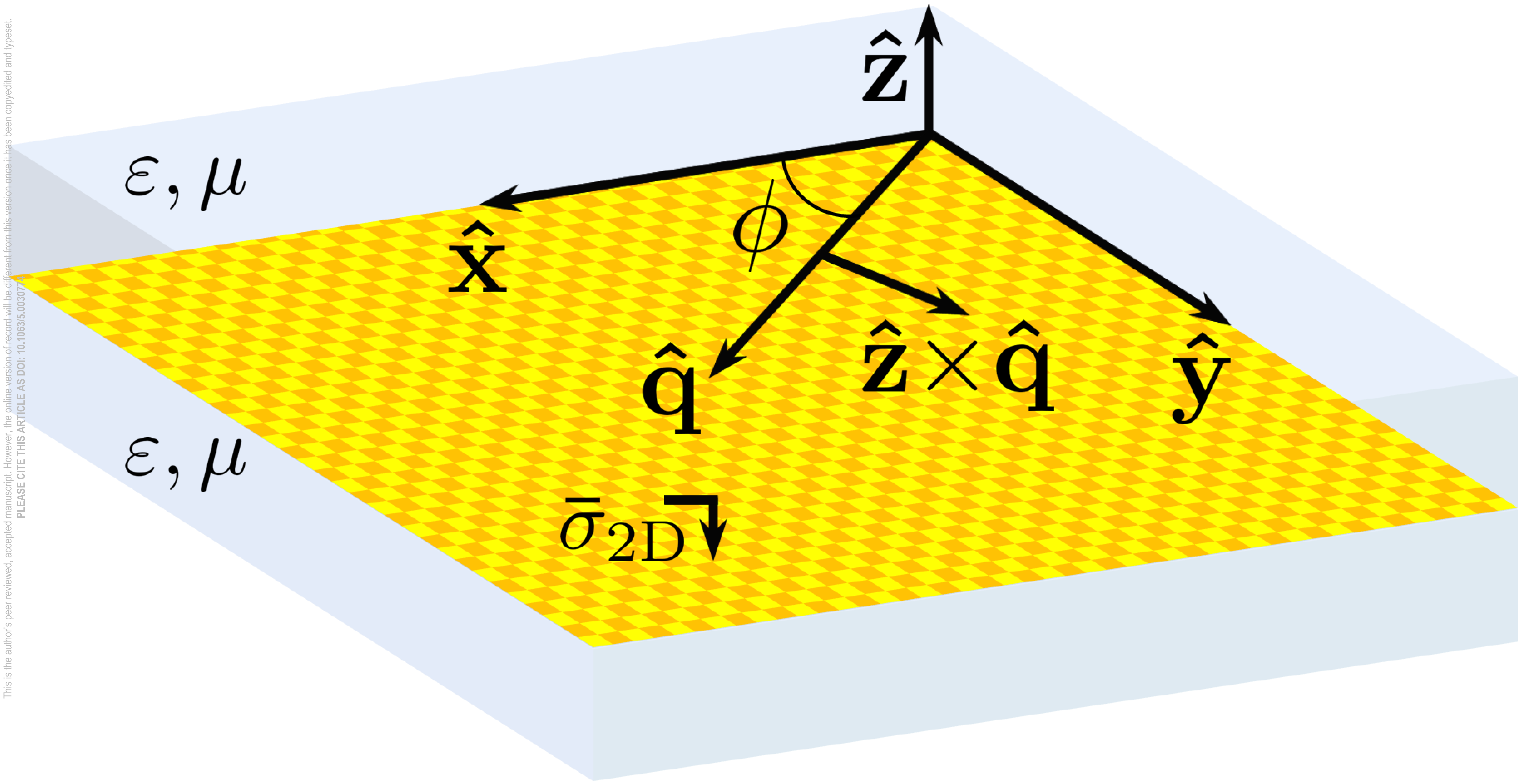
ε, μ
$\hat{\mathbf{z}}$
$\hat{\mathbf{x}}$
ϕ
$\hat{\mathbf{y}}$
$\hat{\mathbf{q}}$
$\hat{\mathbf{z}} \times \hat{\mathbf{q}}$
ε, μ
$\bar{\sigma}_{2\mathrm{D}}$

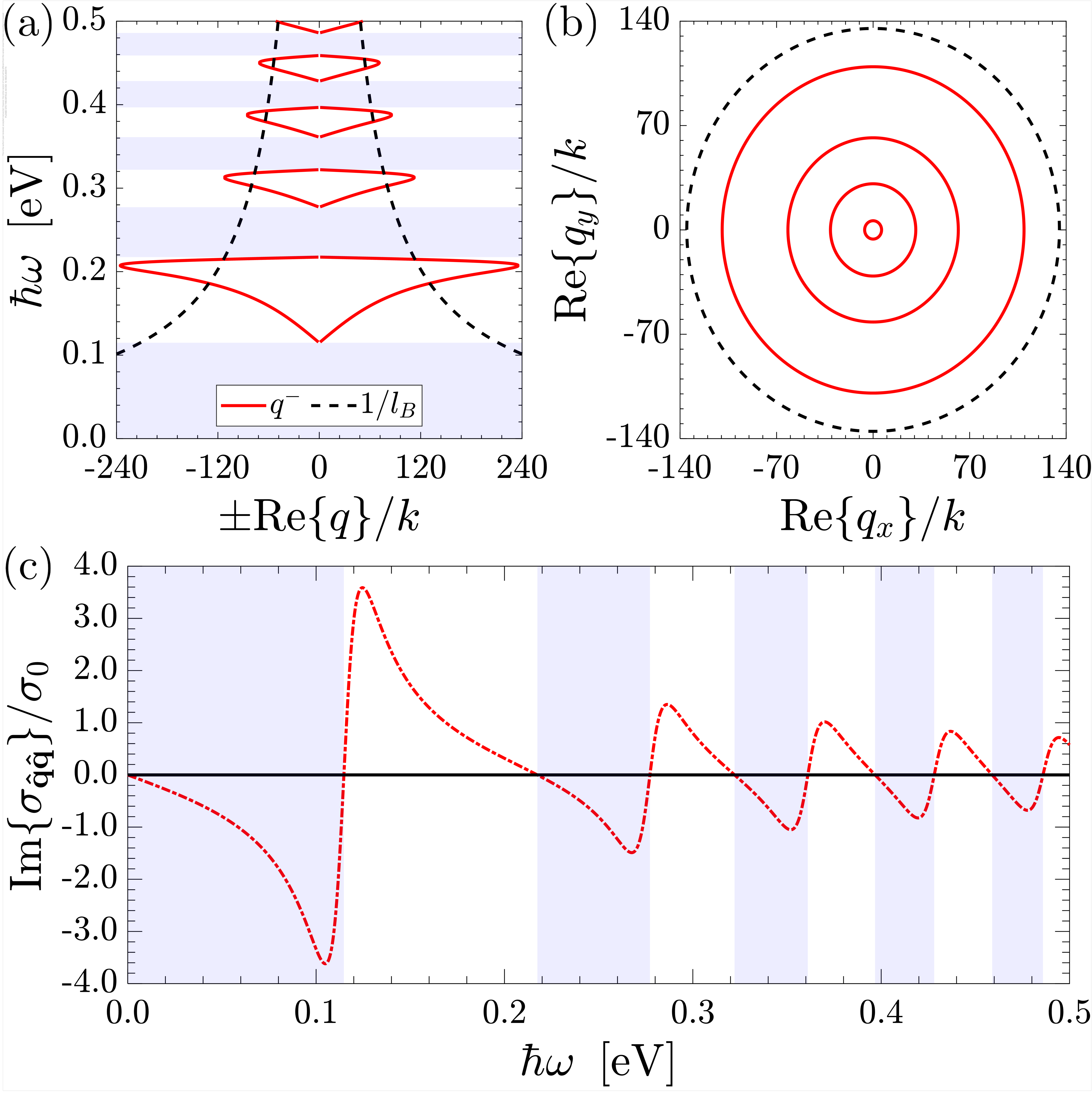
(a)
(b)
(c)
ħω [eV]
±Re{q}/k
q⁻
1/l_B
Re{q_y}/k
Re{q_x}/k
Im{σ_q̂q̂}/σ_0
0.0
0.1
0.2
0.3
0.4
0.5
-240
-120
0
120
240
140
70
-70
-140
4.0
3.0
2.0
1.0
-1.0
-2.0
-3.0
-4.0

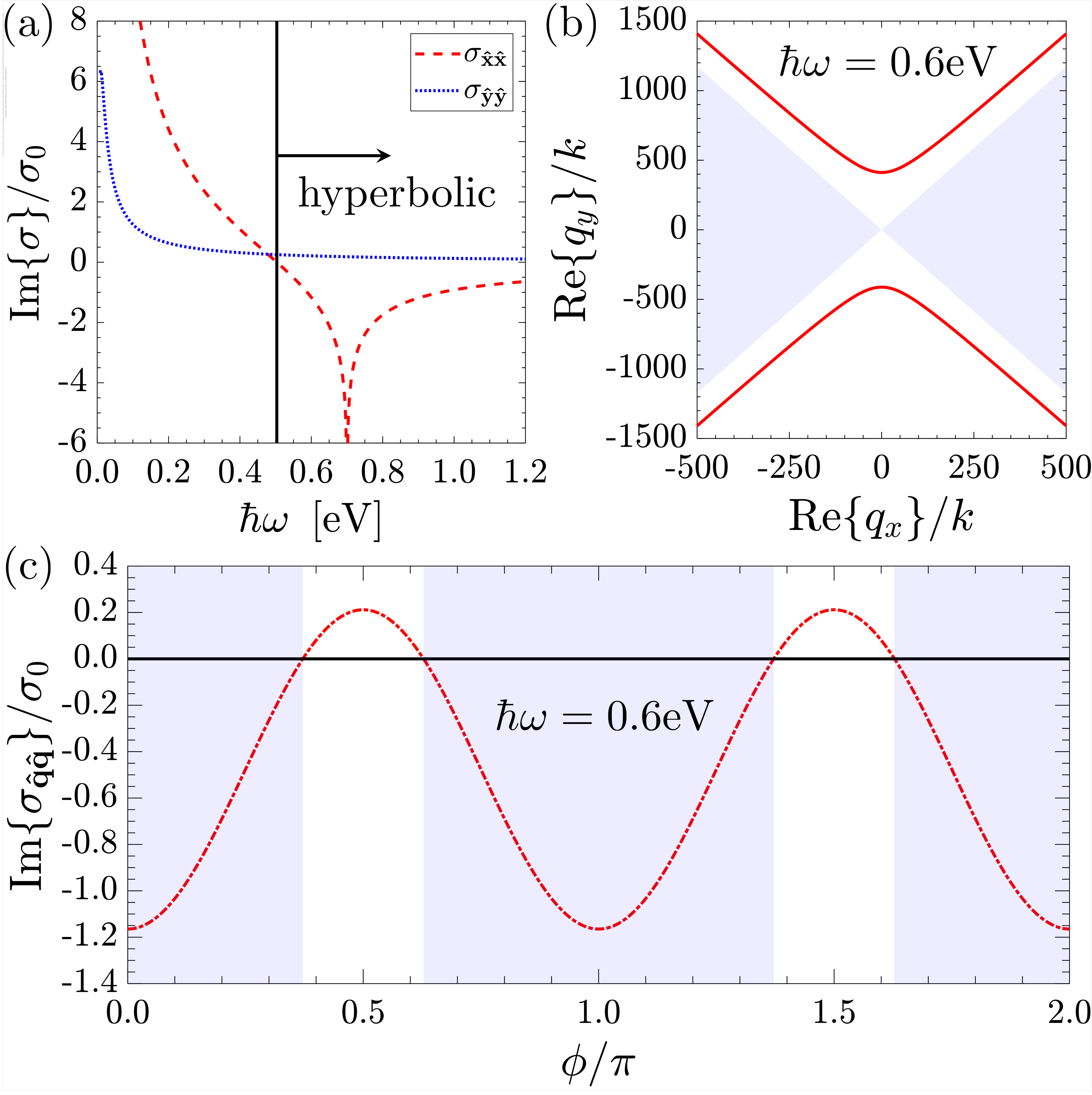
(a)
$\sigma_{\hat{x}\hat{x}}$
$\sigma_{\hat{y}\hat{y}}$
hyperbolic
$\mathrm{Im}\{\sigma\}/\sigma_0$
$\hbar\omega$ [eV]
(b)
$\hbar\omega = 0.6\mathrm{eV}$
$\mathrm{Re}\{q_y\}/k$
$\mathrm{Re}\{q_x\}/k$
(c)
$\hbar\omega = 0.6\mathrm{eV}$
$\mathrm{Im}\{\sigma_{\hat{q}\hat{q}}\}/\sigma_0$
ϕ/π